Self-Adapting Online Loss Minimization of a Dual Active Bridge in Buck and Boost Mode

1st Tobias Merz
Elektrotechnisches Institut (ETI)
Karlsruhe Institute of Technology (KIT)
Karlsruhe, Germany
tobias.merz@kit.edu

2nd Fabian Sommer
Elektrotechnisches Institut (ETI)
Karlsruhe Institute of Technology (KIT)
Karlsruhe, Germany

3rd Nikolas Menger
Elektrotechnisches Institut (ETI)
Karlsruhe Institute of Technology (KIT)
Karlsruhe, Germany

4th Sophie Knierim
Elektrotechnisches Institut (ETI)
Karlsruhe Institute of Technology (KIT)
Karlsruhe, Germany

5th Rüdiger Schwendemann
Elektrotechnisches Institut (ETI)
Karlsruhe Institute of Technology (KIT)
Karlsruhe, Germany

6th Marc Hiller
Elektrotechnisches Institut (ETI)
Karlsruhe Institute of Technology (KIT)
Karlsruhe, Germany

***Abstract*—In this paper, an online self-adapting and self-optimizing algorithm for increased efficiency of a high power Dual Active Bridge (DAB) in Triple Phase Shift buck and boost operation is presented. The algorithm estimates internal losses and performs iterative optimization steps during operation in the direction of the steepest descent, without requiring additional high-precision voltage or current sensors. Due to the working principle of the algorithm it is ensured that only operation points with lower losses are chosen for the next optimization step. Experimental results demonstrate that switching angles derived from precalculated Circular Current Injection method or Triangular Current Mode modulation can be further improved to reduce losses. A loss reduction of approximately 20 % can be achieved using a 450 kW medium voltage DAB testbench.**

***Index Terms*—Optimization, Energy efficiency, DC-DC power converters, Dual Active Bridge, Triple Phase Shift**

I. Introduction

In order to improve the efficiency of a Dual Active Bridge (DAB) in buck and boost operation, two main loss mechanisms are investigated in literature. The conduction losses caused by the root mean square (RMS) current and the resistive part of the AC circuit, as well as the switching losses of the semiconductors. Closed-form equations aimed at improving the modulation scheme to minimize RMS current and thereby reduce conduction losses are presented in [1]. In contrast, other approaches rely on analytical, numerical, and measurement-based methods to derive optimized Triple Phase Shift (TPS) switching patterns that enable zero voltage switching (ZVS) of the semiconductors, thereby reducing switching losses [2]–[7]. A closed-form solution for ZVS modulation was proposed in [8]. More recent works also consider additional effects, such as adapting the switching current based on the nonlinear, voltage-dependent output capacitance [9], accepting higher RMS and peak currents to ensure ZVS [10], or treating the switching frequency as an additional Degree of Freedom (DoF) [11] to extend the ZVS area. In [12], [13] detailed and rigorous mathematical models of the DAB including the transformer winding and core losses are derived and optimized to get the optimal switching angles.

All of the improved TPS modulation techniques with optimized switching angles have in common, that higher AC RMS currents and therefore higher conduction losses are accepted to ensure ZVS for each turn-on transition of the semiconductors.

However, all of these approaches either rely on datasheet values, additional measurements of the existing hardware, or precise mathematical models of the DAB. Aging, temperature effects during operation, and manufacturing deviations are difficult to consider during the life cycle of the system. Nevertheless, the aforementioned aspects significantly impact system behavior, resulting in non-optimal outcomes for offline-optimized methods. In [14], an algorithm was presented that modifies the switching angles of the semiconductors online to improve efficiency based on theoretically derived ZVS and minimum RMS trajectories. The feedback loop for finding the operation point (OP) with maximum efficiency along the algorithm's predefined trajectories is closed using an external power meter (PM).

In this paper, the idea of online optimization is extended to be less restrictive and more applicable to a wider range of uses. Both constraints, achieving ZVS and minimizing RMS current, are relaxed in favor of the overarching objective: minimizing total losses at the requested OP with Triangular Current Mode (TCM) modulation. To further enhance usability, the proposed method does not require an external PM but instead relies entirely on existing sensor data from the DAB. The proposed algorithm builds on the concept of circular current injection (CCI), originally introduced in [15]. Unlike the approach in [15], the circular currents are not derived from datasheet values but are optimized online. Therefore, the method is referred to as Online Optimized Circular Current Injection (OOCCI).

II. Topology

Fig. 1 illustrates the ideal equivalent circuit of a DAB. The DC link voltages are denoted by U_x, and the corresponding

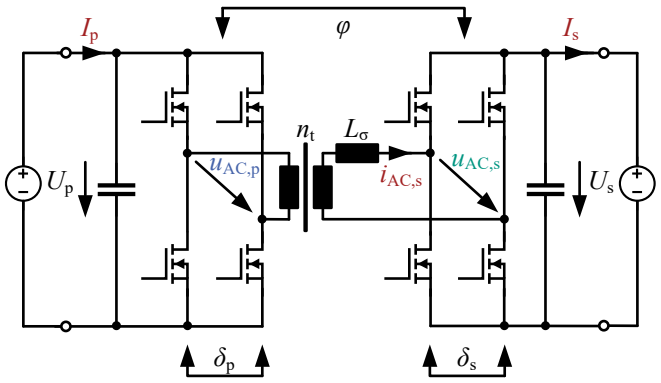

Fig. 1: Idealized equivalent circuit of DAB with constant voltage load.

AC voltages at the transformer terminals by $u_{\mathrm{AC},x}$, where $x \in \{\mathrm{p}, \mathrm{s}\}$. The index 'p' refers to the primary side and 's' to the secondary side of the DAB. The input and output currents are labeled as I_x, while the AC current on the transformer's secondary side is denoted by $i_{\mathrm{AC,s}}$. The AC leakage inductance is L_σ and the transformer's turn ratio is represented by n_t.

The following equations (1)–(3) are used for an ideal DAB to achieve minimum RMS current in the AC circuit with low power buck and boost operation for the desired output current I_s^*. This operating mode, referred to as TCM modulation, is based on the results presented in [16]. The outer phase shift $\varphi \in [-\pi, +\pi]$ between the fundamental components of the AC voltages $u_{\mathrm{AC,p}}$ and $u_{\mathrm{AC,s}}$ is generated by the two full-bridges. It is determined by the output current setpoint I_s^*, the DC link voltages, the leakage inductance L_σ, and the switching frequency f_s, as described in (1). The phase shift within each full-bridge is denoted by δ_x, where $\delta_x = 0$ corresponds to maximum RMS voltage and $\delta_x = \pi$ corresponds to zero output voltage. The resulting ideal voltage and current waveforms for TCM modulation during buck operation with positive output current $I_\mathrm{s} > 0\,\mathrm{A}$ and power flow $P_\mathrm{s} = U_\mathrm{s} \cdot I_\mathrm{s} > 0\,\mathrm{W}$ are illustrated in Fig. 2.

$$\varphi = \mathrm{sign}(I_\mathrm{s}^*) \cdot \sqrt{|I_\mathrm{s}^*|\pi^2 f_\mathrm{s} L_\sigma} \cdot \begin{cases} \sqrt{\frac{n_\mathrm{t}U_\mathrm{p} - U_\mathrm{s}}{n_\mathrm{t}U_\mathrm{p} \cdot U_\mathrm{s}}} & n_\mathrm{t}U_\mathrm{p} > U_\mathrm{s} \\ \sqrt{\frac{U_\mathrm{s} - n_\mathrm{t}U_\mathrm{p}}{(n_\mathrm{t}U_\mathrm{p})^2}} & n_\mathrm{t}U_\mathrm{p} < U_\mathrm{s} \end{cases} \tag{1}$$

$$\delta_\mathrm{p} = \pi - \frac{U_\mathrm{s}}{|n_\mathrm{t}U_\mathrm{p} - U_\mathrm{s}|} \cdot 2 \cdot |\varphi| \tag{2}$$

$$\delta_\mathrm{s} = \pi - \frac{n_\mathrm{t}U_\mathrm{p}}{|n_\mathrm{t}U_\mathrm{p} - U_\mathrm{s}|} \cdot 2 \cdot |\varphi| \tag{3}$$

III. Losses and Parasitics

Parasitic effects have a significant impact on the performance and efficiency of the DAB. While some can be modeled and compensated using nominal datasheet parameters, their actual values often deviate due to manufacturing tolerances, temperature variations, and operating conditions. These additional deviations are difficult to predict yet must be considered alongside the parasitic elements themselves to ensure robust and optimized system operation.

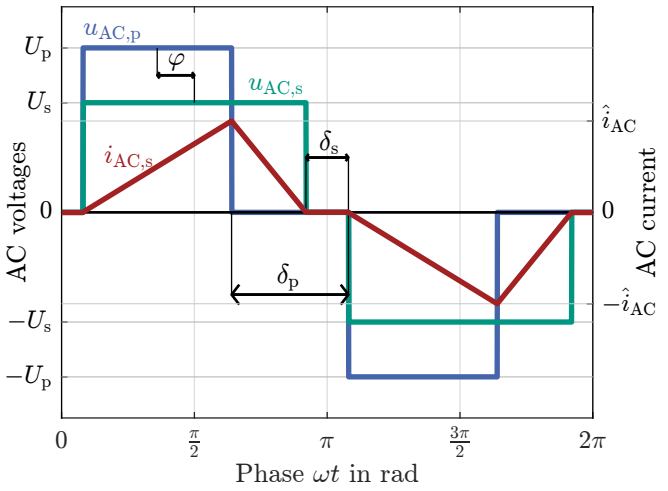

Fig. 2: Ideal current and voltage waveforms with TCM modulation to achieve minimum RMS current for buck operation with positive output power ($n_\mathrm{t}U_\mathrm{p} > U_\mathrm{s}$, $P_\mathrm{s} > 0\,\mathrm{W}$).

A. DAB losses

During the operation of a power electronic system, several predictable effects contribute to the overall power loss. For a DAB in particular, the total power loss can be expressed as the sum of four components, as shown in (4). The conduction losses P_con, given by (5), result from the AC current I_AC flowing through the total series AC resistance R of the semiconductors, transformer windings, and connecting conductors, including their interfaces. Switching losses P_sw, defined in (6), occur during the turn-on and turn-off transitions of the eight semiconductors. Iron losses P_iron, described by (7), originate in the transformer core and are caused by eddy currents and magnetic hysteresis effects based on material constants [17], [18]. These three components typically represent the dominant contributions to the total power loss [9] and can be estimated using datasheet parameters and empirical data, supplementary measurements, and analytical models. For instance, a detailed analysis of (5)-(7) for improved switching angles of the DAB to minimize the loss function is done in [13].

However, the fourth component of (4), denoted as the additional loss term P_add, is not explicitly considered in the optimization. This term is difficult to quantify and cannot be clearly assigned to a single physical mechanism. In this work, it represents all deviations from the expected losses caused by model inaccuracies, unmodeled parasitic effects that lead to different voltage and current waveforms, and measurement uncertainties. The key contribution of this paper is to inherently include these additional parasitic or deviating loss effects, detailed in the following section, in the optimization process.

$$P_\mathrm{loss} = P_\mathrm{con} + P_\mathrm{sw} + P_\mathrm{iron} + P_\mathrm{add} \tag{4}$$

$$P_\mathrm{con} = R \cdot I_\mathrm{AC}^2 \tag{5}$$

$$P_{\mathrm{sw}} = \frac{1}{f_{\mathrm{sw}}} \int_{t_{\mathrm{on}}} u_{\mathrm{on}}(t) \cdot i_{\mathrm{on}}(t) \mathrm{d}t + \frac{1}{f_{\mathrm{sw}}} \int_{t_{\mathrm{off}}} u_{\mathrm{off}}(t) \cdot i_{\mathrm{off}}(t) \mathrm{d}t \tag{6}$$

$$P_{\mathrm{iron}} = \left(C_{\mathrm{m}} f_{\mathrm{eq}}^{\alpha-1} \hat{B}^{\beta} \right) f_{\mathrm{r}} \tag{7}$$

B. Additional parasitic effects

Offline calculations and optimizations are inherently prone to inaccuracies, as they rely on expected datasheet parameters and presumably correctly measured values of the test setup. However, several factors cause deviations of the real hardware from the mathematically modeled system in software.

1) Resistive effects: The copper resistance of the AC circuit is temperature dependent and increases by approximately $25\,\%$ for a temperature rise of $\Delta T = 65\,\mathrm{K}$. In addition, the on-state resistance of the semiconductors $r_{\mathrm{DS,on}}$ can increase by up to $120\,\%$ over the full temperature range [19], [20]. Both effects directly influence the conduction losses but also cause a superimposed exponential decay of the transformer AC current i_{AC}. This change in the current waveform in turn affects the switching losses.

2) Transformer deviations: Manufacturing tolerances combined with temperature-dependent variations of the transformer's AC inductance L_{σ} can lead to deviations of more than $\pm 20\,\%$ [21]–[23]. For highly utilized transformers, saturation effects may additionally alter the effective AC inductance at high current levels. Depending on the OP and the AC voltages on both sides, the superimposed magnetizing current in the transformer's main inductance also affects the semiconductor switching behavior. Moreover, additional losses may arise from eddy currents in the transformer case or in nearby conductive materials exposed to varying magnetic fields radiated by the connection wires.

3) Deviations in the commutation capacitance: The equivalent commutation capacitance C_{eq} of the semiconductors, and therefore the charge Q_{eq} required to achieve ZVS, depend on the operating voltage [8], [19], [20]. However, since an infinitely high resolution cannot be realized in the lookup table (LUT), discretization errors are introduced when storing the offline optimized switching angles across the entire voltage operating range of the DAB.

4) Commutation effects of the semiconductors: The commutation behavior of the semiconductors depends on the drain current [19], [20] and varies with temperature due to changes in transition times and threshold voltages [20], [24], [25]. Additional timing mismatches between the primary and secondary gate drivers further influence the effective inner and outer switching angles, resulting in deviations from the expected current and voltage waveforms.

5) Measurement errors: Inaccuracies in the measurement system, particularly in the voltage and current sensing circuits, can lead to errors when reading-out and applying the offline-optimized switching angles during operation.

IV. Concept

In this chapter, the principle of the self-adapting algorithm for online loss minimization for TCM modulation is presented. The concept is based on a systematic modification of the DAB's switching angles, followed by a comparison of the estimated power losses using measured DC system data. A superimposed controller compensates for the angle variations and ensures that the transmitted output current and power remain at their desired values. In contrast to previous publications [1], [7]–[11], [15], the proposed self-adapting method does not require additional measurements or offline-optimized, highly accurate mathematical models. Moreover, it eliminates the need for external measurement equipment, such as the PM used in [14], to determine the expected point of maximum efficiency. In general, the OOCCI algorithm does not explicitly aim to minimize specific loss components, such as conduction or turn-on losses, but rather the total power losses irrespective of their origin.

A. Power loss estimation

To avoid the necessity for a precise external PM, inherently available measured sensor data for voltage and current are used to estimate (marked with '$\sim$') the power $\tilde{P}_x$ on both sides of the DAB as shown in (8). Although the measured values ('m' index) are subject to errors of offset, gain and nonlinearity, this method remains valid if the transfer function of the measured values exhibits strict monotonic behavior. This means, that a higher physical value has to have a higher digital representation and vice versa. Additional inevitably superimposed measurement noise can also be neglected since digital filters can be used during the optimization process of the quasi-stationary OP. Without loss of generality only positive output current and power are considered in the following. Consequently, the relation $|P_{\mathrm{p}}| \geq |P_{\mathrm{s}}|$ holds.

$$\tilde{P}_x = U_{x,\mathrm{m}} \cdot I_{x,\mathrm{m}} \tag{8}$$

The optimization objective is to minimize the estimated power losses $\tilde{P}_{\mathrm{loss}}$, which are obtained from the difference between estimated input and output power, as expressed in (9) while keeping the output current I_{s} at its setpoint value.

$$\tilde{P}_{\mathrm{loss}} = \tilde{P}_{\mathrm{p}} - \tilde{P}_{\mathrm{s}} = U_{\mathrm{p,m}} \cdot I_{\mathrm{p,m}} - U_{\mathrm{s,m}} \cdot I_{\mathrm{s,m}} \tag{9}$$

B. Modification of switching angles

For the investigated operation of the DAB, both voltages U_{p} and U_{s} are assumed to be quasi-stationary and they are regulated by external voltage sources, while the output current I_{s} is directly controlled by the converter. Hence, reducing the primary current I_{p} also corresponds to minimizing $\tilde{P}_{\mathrm{loss}}$ and therefore increasing the efficiency $\eta_{\mathrm{DAB}}(U_{\mathrm{p}}, U_{\mathrm{s}}, I_{\mathrm{s}})$ at this OP.

To reduce the losses, the switching angles φ and δ_x can be modified. This is done by adding offsets $\Delta\varphi$ and $\Delta\delta_x$, as shown in (10) and (11), respectively. These offsets represent intended deviations from the ideal TCM modulation equations. Exemplary modified voltage and current waveforms are shown in Fig. 3. As explained in [15], changing φ and either δ_{p} on

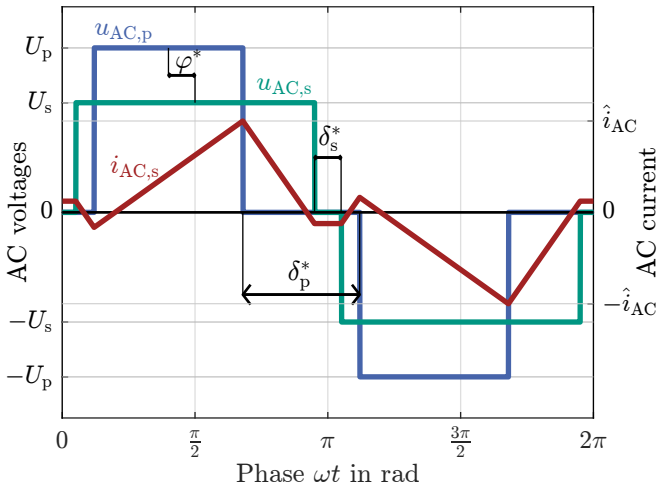

Fig. 3: Current and voltage waveforms with modified TCM modulation to achieve lower losses in buck operation with positive output power ($n_t U_p > U_s$, $P_s > 0\,\mathrm{W}$).

boost ($n_t U_p < U_s$) or δ_s in buck mode ($n_t U_p > U_s$) allows for adjusting the switching currents of the semiconductors independently. This modification uses two of the three DoF in shaping the current waveform. The third DoF is necessary to control the output power.

$$\varphi^* = \varphi + \Delta\varphi \tag{10}$$

$$\delta_x^* = \delta_x + \Delta\delta_x \tag{11}$$

C. Optimization process

To realize this optimization in a computationally efficient manner, a steepest descent algorithm is employed to minimize the estimated losses $\tilde{P}_{\mathrm{loss}}$. The algorithm iteratively adjusts the switching angles by applying a modification vector to the initial angles derived from TCM modulation, expressed as $\boldsymbol{\theta}_0^{(k)} = (\Delta\varphi^{(k)}, \Delta\delta_x^{(k)})^{\mathrm{T}}$ where k denotes the iteration index of the optimization process. The procedure is illustrated in the flowchart in Fig. 4 and detailed below.

1) Estimate the power losses $\tilde{P}_{\mathrm{loss}}(\boldsymbol{\theta}_0^{(k)})$ at the initial switching angle modification vector $\boldsymbol{\theta}_0^{(k)}$.
2) Apply the variation vector $\mathbf{m} = m \cdot \vec{\mathrm{e}}_1 = (m, 0)^{\mathrm{T}}$ to the initial point. Estimate $\tilde{P}_{\mathrm{loss}}(\boldsymbol{\theta}_1^{(k)})$.
3) Apply a second, linearly independent variation $\mathbf{n} = n \cdot \vec{\mathrm{e}}_2 = (0, n)^{\mathrm{T}}$. Estimate $\tilde{P}_{\mathrm{loss}}(\boldsymbol{\theta}_2^{(k)})$.
4) Approximate the local steepest descent direction $\mathbf{p}_{\mathrm{temp}}^{(k)}$:

$$\mathbf{p}_{\mathrm{temp}}^{(k)} = -\sum_{d=1}^{2} \frac{\tilde{P}_{\mathrm{loss}}(\boldsymbol{\theta}_d^{(k)}) - \tilde{P}_{\mathrm{loss}}(\boldsymbol{\theta}_0^{(k)})}{|\boldsymbol{\theta}_d^{(k)} - \boldsymbol{\theta}_0^{(k)}|} \cdot \vec{\mathrm{e}}_d \tag{12}$$

Limit the maximum length of $\mathbf{p}_{\mathrm{temp}}^{(k)}$ to $|\mathbf{m}+\mathbf{n}|$:

$$\mathbf{p}^{(k)} = \mathbf{p}_{\mathrm{temp}}^{(k)} \cdot \begin{cases} 1 & \text{for } |\mathbf{p}_{\mathrm{temp}}^{(k)}| \le |\mathbf{m}+\mathbf{n}| \\ \frac{|\mathbf{m}+\mathbf{n}|}{|\mathbf{p}_{\mathrm{temp}}^{(k)}|} & \text{for } |\mathbf{p}_{\mathrm{temp}}^{(k)}| > |\mathbf{m}+\mathbf{n}| \end{cases} \tag{13}$$

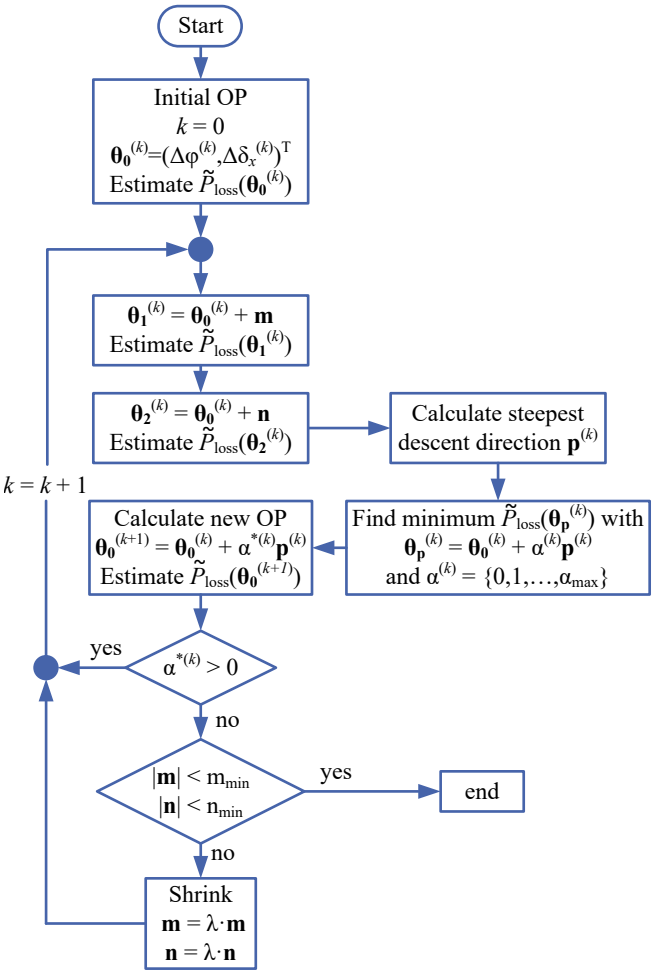

Fig. 4: Flowchart of the steepest descent OOCCI optimization algorithm.

5) Vary $\alpha^{(k)}$ over the set of values $\alpha^{(k)} = \{0, 1, \ldots, \alpha_{\max}\}$ until a local minimum of $\tilde{P}_{\mathrm{loss}}(\boldsymbol{\theta}_{\mathrm{p}}^{(k)})$ is found along $\mathbf{p}^{(k)}$:

$$\boldsymbol{\theta}_{\mathrm{p}}^{(k)} = \boldsymbol{\theta}_0^{(k)} + \alpha^{(k)} \cdot \mathbf{p}^{(k)} \tag{14}$$

6) Update the current best switching angle modification with the $\alpha^{*(k)}$ that lead to the local minimum along $\mathbf{p}^{(k)}$ and estimate $\tilde{P}_{\mathrm{loss}}(\boldsymbol{\theta}_0^{(k+1)})$.
7) If $\alpha^{*(k)} > 0$, increment k by 1 and go to step 2.
8) If $|\mathbf{m}| < m_{\min}$ and $|\mathbf{n}| < n_{\min}$, the algorithm terminates.
9) If the termination condition is not met, multiply the variation vectors with the factor $0 < \lambda < 1$.
10) Increment k by 1 and return to step 2.

The parameters m, n, $m_{\min}$, $n_{\min}$, $\alpha_{\max}$ and λ used in the algorithm represent tuning variables that require appropriate configuration to ensure efficient convergence.

If the algorithm terminates, the resulting switching angle modification vector $\boldsymbol{\theta}_0^{(k+1)}$ leads to the estimated loss minimum. As operating conditions such as temperature and output power of the DAB vary continuously, the algorithm should be executed repeatedly. Using the previously determined optimal vector as the new initial guess improves convergence.

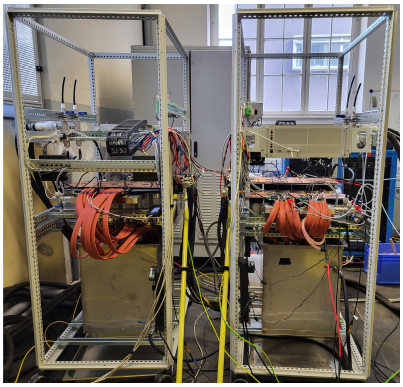

Fig. 5: Two 450 kW DABs configured in a B2B setup.

TABLE I
Parameters of the MV DAB referred to the secondary side.

Parameter	Symbol	Value
Nominal output power	P_{nom}	450 kW
Primary voltage range	U_{p}	560 V – 800 V
Secondary voltage range	$U_{\mathrm{s,max}}$	1400 V – 2000 V
Maximum output current	$I_{\mathrm{s,max}}$	±250 A
FPGA clock frequency	f_{FPGA}	150 MHz
Switching and control frequency	f_{sw}	15 kHz
Semiconductors primary side	FMF1200DXZ-24B	
Semiconductors secondary side	FMF750DC-66A	
Transformer winding ratio	n_{t}	1 : 2.5
Leakage inductance	L_{σ}	9.0 µH

V. Test Bench

Fig. 5 shows the test bench with a back-to-back (B2B) setup using two DABs. Each DAB includes both the power stage and its associated measurement and control electronics. The real-time control algorithm, as explained in [26], is implemented on an field-programmable gate array (FPGA) with a clock frequency of $f_{\mathrm{FPGA}} = 150\,\mathrm{MHz}$. One DAB controls the LV side voltage U_{p}. The other DAB, which is the Device Under Test (DUT), has OOCCI implemented. The tuning parameters of the algorithm are set as follows: $m = 16$, $n = 16$, $m_{\mathrm{min}} = 2$, $n_{\mathrm{min}} = 2$, $\alpha_{\mathrm{max}} = 6$ and $\lambda = 0.5$. The DUT controls the output current I_{s} on the MV side. This also determines the transmitted output power P_{s}. The voltage on the secondary side U_{s} is controlled by a power supply. To validate the results, a Gen7tA PM by *HBM* is used to measure the efficiency of the DAB. In Table I the most relevant data of the DABs are summarized.

VI. Experimental Results

To evaluate the performance of OOCCI, power losses were measured using a PM across a relevant region of the $(\Delta\varphi,\ \Delta\delta_x)$-plane, specifically for $-80 \leq \Delta\varphi \leq 10$ and $-120 \leq \Delta\delta_{\mathrm{s}} \leq 10$, with a step size of 5 in each direction. These values represent clock cycles of the FPGA and therefore time steps $t_{\mathrm{FPGA}} = \frac{1}{f_{\mathrm{FPGA}}}$. Fig. 6 shows these reference measurements as the colored background, along with the experimental results obtained using OOCCI at an OP of $U_{\mathrm{p}} = 720\,\mathrm{V}$, $U_{\mathrm{s}} = 1620\,\mathrm{V}$, and $I_{\mathrm{s}} = 50\,\mathrm{A}$. Since the converter operates in buck mode with positive power, $\Delta\delta_{\mathrm{p}}$ is set to zero, while $\Delta\delta_{\mathrm{s}}$ is varied [15].

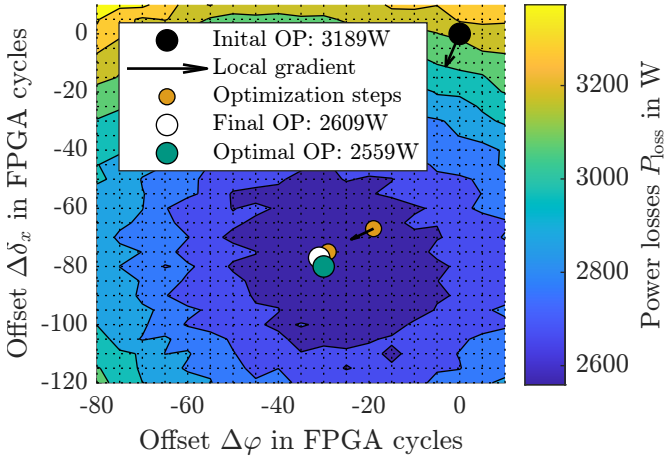

Fig. 6: Optimization process with OOCCI at $U_{\mathrm{p}} = 720\,\mathrm{V}$, $U_{\mathrm{s}} = 1620\,\mathrm{V}$ and $I_{\mathrm{s}} = 50\,\mathrm{A}$. Here, $\Delta\delta_x = \Delta\delta_{\mathrm{s}}$.

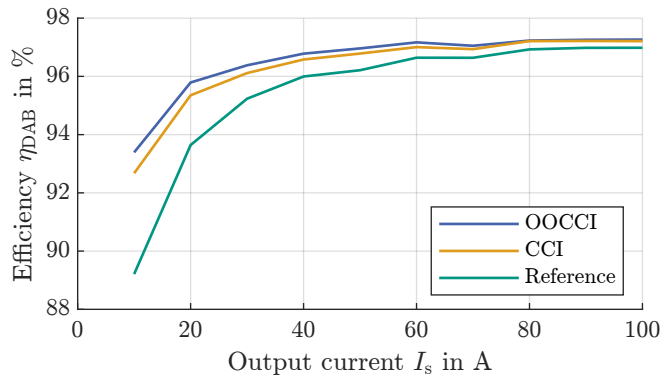

Fig. 7: Efficiency curve with OOCCI, CCI and unmodified reference at $U_{\mathrm{p}} = 720\,\mathrm{V}$, $U_{\mathrm{s}} = 1620\,\mathrm{V}$ and up to $P_{\mathrm{s}} = 162\,\mathrm{kW}$.

The online optimization process starts at the initial OP with $\Delta\varphi = \Delta\delta_x = 0$, marked in black, corresponding to measured power losses of $P_{\mathrm{loss}} = 3189\,\mathrm{W}$. The subsequent optimization steps are illustrated in orange. Although the algorithm relies exclusively on internal sensor data, the final OP, highlighted in white, achieves power losses of $P_{\mathrm{loss}} = 2609\,\mathrm{W}$, which is within 2 % of the global optimum of $P_{\mathrm{loss}} = 2559\,\mathrm{W}$, indicated in green. The optimized OP therefore achieves a loss reduction of approximately 20 % compared to the initial OP calculated with the TCM equations. Consequently, the efficiency improves from $\eta_{\mathrm{DAB,init}} \approx 96.2\,\%$ to $\eta_{\mathrm{DAB,OOCCI}} \approx 96.9\,\%$.

In practice, the OP of the DAB varies with the application's power demand. However, if voltage and current change gradually, for example during the charging cycle of an electric vehicle (EV), the currently optimized modification vector defined by $\Delta\varphi$ and $\Delta\delta_x$ can be used as the initial condition for the next optimization cycle.

Fig. 7 shows the efficiency curves of OOCCI, CCI, and the unmodified reference for $U_{\mathrm{p}} = 720\,\mathrm{V}$ and $U_{\mathrm{s}} = 1620\,\mathrm{V}$. While the analytical CCI approach [15] consistently outperforms the reference, the proposed OOCCI achieves an even higher efficiency across the entire operating range.

VII. Conclusion

This paper presented an easy-to-implement, self-adapting online optimization algorithm for improving the efficiency of DABs under real operating conditions. The proposed OOCCI algorithm systematically adjusts the switching angles during operation, relying solely on inherently available sensor data. It does not require offline calculations, high-precision sensors, or external measurement equipment.

By minimizing the total power losses rather than focusing on individual loss components, the algorithm inherently accounts for parasitic effects such as temperature-induced resistance changes, transformer manufacturing tolerances, and variations in semiconductor switching behavior. Experimental results obtained from a $450\,\mathrm{kW}$ DAB test bench demonstrate that the algorithm can reduce total losses by up to $20\,\%$.

The resulting optimized OP is within $2\,\%$ of the global optimum identified through reference PM measurements, confirming the effectiveness of the proposed self-optimizing approach. Owing to its simplicity, robustness, and adaptability, the method is well suited for implementation in practical converter applications such as EV chargers and grid applications.

Future work will focus on extending the approach to other DAB modulation strategies, evaluating its robustness against measurement errors, and investigating its convergence behavior from different initial operating conditions.

Acknowledgment

The authors gratefully acknowledge funding by the German Federal Ministry of Research, Technology and Space (BMFTR) within the Kopernikus Project ENSURE 'New ENergy grid StructURes for the German Energiewende'.

References

[1] F. Krismer and J. W. Kolar, "Closed form solution for minimum conduction loss modulation of DAB converters," *IEEE Transactions on Power Electronics*, vol. 27, no. 1, pp. 174–188, 2012.

[2] G. G. Oggier, G. O. Garcia, and A. R. Oliva, "Modulation strategy to operate the dual active bridge DCDC converter under soft switching in the whole operating range," *IEEE Transactions on Power Electronics*, vol. 26, no. 4, pp. 1228–1236, 2011.

[3] J. Everts, J. Van Den Keybus, F. Krismer, J. Driesen, and J. W. Kolar, "Switching control strategy for full ZVS soft-switching operation of a dual active bridge AC/DC converter," *Conference Proceedings - IEEE Applied Power Electronics Conference and Exposition - APEC*, pp. 1048–1055, 2012.

[4] F. Krismer and J. W. Kolar, "Efficiency-optimized high-current dual active bridge converter for automotive applications," *IEEE Transactions on Industrial Electronics*, vol. 59, no. 7, pp. 2745–2760, 2012.

[5] J. Everts, F. Krismer, J. Van Den Keybus, J. Driesen, and J. W. Kolar, "Charge-based ZVS soft switching analysis of a single-stage dual active bridge AC-DC converter," *2013 IEEE Energy Conversion Congress and Exposition, ECCE 2013*, pp. 4820–4829, 2013.

[6] ——, "Optimal zvs modulation of single-phase single-stage bidirectional dab ac-dc converters," *IEEE Transactions on Power Electronics*, vol. 29, no. 8, pp. 3954–3970, 2014.

[7] Y. Yan, H. Bai, A. Foote, and W. Wang, "Securing Full-Power-Range Zero-Voltage Switching in Both Steady-State and Transient Operations for a Dual-Active-Bridge-Based Bidirectional Electric Vehicle Charger," *IEEE Transactions on Power Electronics*, vol. 35, no. 7, pp. 7506–7519, 2020.

[8] J. Everts, "Closed-Form Solution for Efficient ZVS Modulation of DAB Converters," *IEEE Transactions on Power Electronics*, vol. 32, no. 10, pp. 7561–7576, 2017.

[9] L. Gong, X. Jin, J. Xu, Z. Deng, H. Li, T. B. Soeiro, and Y. Wang, "A Dynamic ZVS-Guaranteed and Seamless-Mode-Transition Modulation Scheme for the DAB Converter That Maximizes the ZVS Range and Lowers the Inductor RMS Current," *IEEE Transactions on Power Electronics*, vol. 37, no. 11, pp. 13 119–13 134, 2022.

[10] J. Li, Q. Luo, D. Mou, Y. Wei, and X. Zhang, "Comprehensive Optimization Modulation Scheme of Low Current Level and Wide ZVS Range for Dual Active Bridge Converter with Dead-Zone Control," *IEEE Transactions on Power Electronics*, vol. 37, no. 3, pp. 2731–2748, 2022.

[11] D. Lyu, C. Straathof, T. B. Soeiro, Z. Qin, and P. Bauer, "Dual Active Bridge Converter With Variable Switching Frequency Modulation to Maintain ZVS," *2023 25th European Conference on Power Electronics and Applications, EPE 2023 ECCE Europe*, pp. 1–6, 2023.

[12] G. Jean-Pierre, N. Altin, A. El Shafei, and A. Nasiri, "Overall Efficiency Improvement of a Dual Active Bridge Converter Based on Triple Phase-Shift Control," *Energies*, vol. 15, no. 19, pp. 1–28, 2022.

[13] K. Furukawa, Y. Mabuchi, T. Shimada, H. Miyata, M. Ichinose, and K. Gorai, "Triple Phase Shift Modulation Strategy Optimized Losses of Semiconductor Devices and Transformer for DAB Converters," *2025 Energy Conversion Congress and Expo Europe (ECCE Europe)*, vol. 2, 2025.

[14] S. Pistollato, N. Zanatta, T. Caldognetto, and P. Mattavelli, "A low complexity algorithm for efficiency optimization of dual active bridge converters," *IEEE Open Journal of Power Electronics*, vol. 2, no. January, pp. 18–32, 2021.

[15] F. Sommer, T. Merz, R. Schwendemann, and M. Hiller, "Improved Modulation Scheme for a Dual Active Bridge to ensure complete ZVS operation utilizing Circular Currents," *2024 IEEE Energy Conversion Congress and Exposition (ECCE)*, pp. 2634–2641, 2024.

[16] N. Schibli, "Symmetrical Multilevel Converters with two Quadrant DC-DC Feeding," Ph.D. dissertation, EPFL, 2000.

[17] C. P. Steinmetz, "On the law of hysteresis," *Transactions of the American Institute of Electrical Engineers*, vol. 20, pp. 51–57, 1902.

[18] J. Reinert, A. Brockmeyer, and R. W. De Doncker, "Calculation of losses in ferro- and ferrimagnetic materials based on the modified Steinmetz equation," *IEEE Transactions on Industry Applications*, vol. 37, no. 4, pp. 1055–1061, 2001.

[19] MITSUBISHI ELECTRIC CORPORATION, "Datasheet FMF1200DXZ-24B," pp. 1–13, 2022.

[20] ——, "Datasheet FMF750DC-66A," pp. 1–8, 2019.

[21] S. Saeed, J. Garcia, M. S. Perdigao, V. S. Costa, and R. Georgious, "Evaluation of temperature effect on inductance computation in variable magnetic components for Dual-Active-Bridge application," *ECCE 2020 - IEEE Energy Conversion Congress and Exposition*, pp. 3286–3292, 2020.

[22] Z. Guo, Y. Luo, and K. Sun, "Parameter Identification of the Series Inductance in DAB Converters," *IEEE Transactions on Power Electronics*, vol. 36, no. 7, pp. 7395–7399, 2021.

[23] T. Q. Duong and S. J. Choi, "Deadbeat Control With Bivariate Online Parameter Identification for SPS-Modulated DAB Converters," *IEEE Access*, vol. 10, pp. 54 079–54 090, 2022.

[24] J. Lu, K. Sun, H. Wu, Y. Xing, and L. Huang, "Modeling of SiC MOSFET with temperature dependent parameters and its applications," *Conference Proceedings - IEEE Applied Power Electronics Conference and Exposition - APEC*, pp. 540–544, 2013.

[25] K. Tian, J. Qi, Z. Mao, S. Yang, W. Song, M. Yang, and A. Zhang, "Characterization of 1.2 kV 4H-SiC power MOSFETs and Si IGBTs at cryogenic and high temperatures," *2017 14th China International Forum on Solid State Lighting: International Forum on Wide Bandgap Semiconductors China, SSLChina: IFWS 2017*, vol. 2018-Janua, pp. 140–143, 2017.

[26] G. Zieglmaier, F. Sommer, T. Merz, and M. Hiller, "Highly Dynamic Voltage Control of a Dual Active Bridge over the Full Voltage Range by Operating Point Dependent Manipulated Variable Limitation," in *PCIM Europe 2022; International Exhibition and Conference for Power Electronics, Intelligent Motion, Renewable Energy and Energy Management*, vol. 2023-May. VDE, 2023.